Article

Analysis of Factors of Productivity of Tight Conglomerate Reservoirs Based on Random Forest Algorithm

Zhichao Yu, Zhizhang Wang,* Qingping Jiang, Jie Wang, Jingrong Zheng, and Tianyou Zhang

Read Online

ACCESS | Metrics & More | Article Recommendations

ABSTRACT: The tight conglomerate reservoir of Baikouquan formation in the MA 131 well block in the Junggar basin abounds with petroleum reserves, yet the vertical wells in this reservoir have achieved a limited development effect. The tight conglomerate reservoirs have become an important target for exploration and exploitation. The high-efficiency development scheme of a small well spacing three-dimensional (3D) staggered well pattern has been determined by a series of field tests on well pattern and well spacing development. Multistage fracturing with a horizontal well has been demonstrated as the primary development technology. The horizontal wells in the MA 131 small well spacing demonstration area have achieved significantly different development effects, and the major controlling factors for high and stable production of a single well remain unclear. In this study, we proposed an evaluation model of major productivity controlling factors of the tight conglomerate reservoir to provide a reference for oil recovery based on a random forest (RF) machine-learning algorithm. The productivity factors were investigated from two aspects: petrophysical facies that are capable of indicating the genetic mechanism of geological dessert and engineering dessert parameters forming complex fracture networks. Resultantly, the reservoir in the MA 131 well block can be classified into 12 petrophysical facies according to the sedimentary characteristics and diagenesis analysis. The mercury injection curves of a variety of petrophysical facies can be classified into four reservoir quality types. The RF model was trained on 80% of the data to predict the oil well class using the selected features as primary inputs while the remaining 20% of the data were set to test the model performance. The results indicated that the RF model produced excellent results with only 12 misclassifications across the entire data set of 627 samples that represent <2% error. The important evaluation score of the random forest algorithm model showed that the reservoir type, oil saturation, horizontal stress difference, and gravel content are the most important four indicators, with each value exceeding 15%. Brittleness and maximum horizontal stress are considered the least important indexes, with values of less than 5%. Reservoir quality and oil saturation were confirmed as the major controlling factors and material foundation for oil wells' high and stable production. As indicated in this study, stress difference and gravel content are the major controlling factors in the formation of a complex fracture network.
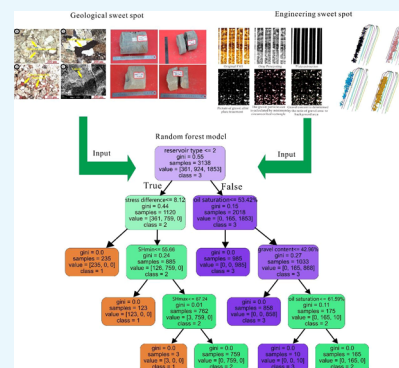
1. INTRODUCTION

China has a wide distribution of tight oil and gas resources in the Junggar, Ordos, Sichuan, and Songliao basins. Exploration and development of tight oil and gas resources show a broad prospect. These resources are currently a new hotspot in global unconventional oil and gas development after shale gas.[1−13] As relevant technologies (e.g., volumetric fracturing and long horizontal well) have been advancing, tight oil and gas resources are expected to be a vital alternative of oil and gas to supply China's high dependence on crude oil and ensure national energy security.[14−16] Global energy consumption is a vital input to many analyses of economic, energy, and environmental policies.[17,18] Over the past few years, the Mahu oilfield in Junggar Basin has been discovered as an extremely large tight conglomerate oil field, which is guided by the accumulation model of a large shallow water retrogradation fan delta in the depression area.[19−21] Typically, marine tight oil or shale oil is characterized by stable deposition, simple

structure, moderate burial depth, and high oil saturation. Moreover, the Mahu tight conglomerate oil reservoir belongs to the fluvial facies fan delta sedimentary system with near-source and rapid accumulation.[22,23] The reservoir has a low effective production rate as a result of the overall complex lithology, poor physical properties, fast lateral variation of the reservoir, low oil saturation, lack of natural fracture development, and significant horizontal stress difference. The "horizontal well with multistage fracturing" small well spacing stereo staggered well pattern of the high-efficiency develop-
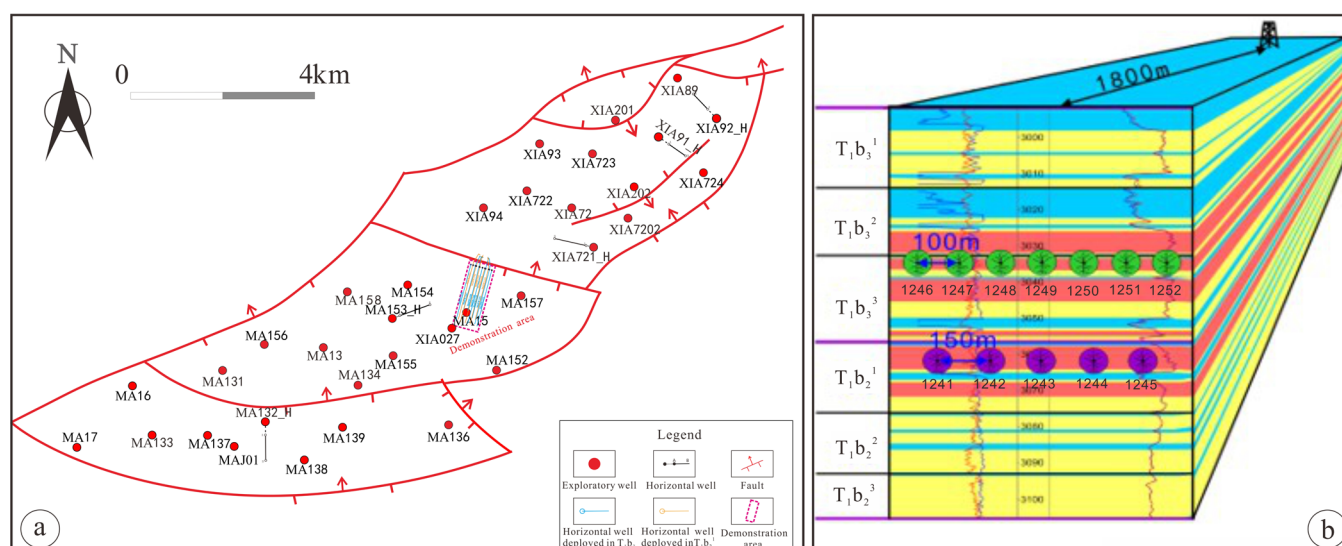
A

Figure 1. (a) Well location map of the MA 131 block and the demonstration area (outlined by the pink line). (b) Schematic diagram of stereo development in the demonstration area (modified after Li 2021).

ment plan was finally obtained through several well types and well spacing tests (e.g., vertical wells with advanced water injection, vertical wells depleting development with water injection, horizontal wells with large spacing, as well as horizontal wells with small spacing). A preferable development effect has been achieved in the demonstration area with small well spacing in the MA 131 block.[24,25] Based on the special characteristics of tight conglomerate development, several development theories have been proposed (e.g., "fracture forming around gravel" and "active interference between wells"). In the study area, the productivity of horizontal wells has been primarily impacted by geological sweet spots and engineering sweet spots. The existing analysis of major controlling factors of productivity has revealed three major problems. (1) For the geological sweet spots, reservoir quality parameters are largely considered, and the formation mechanism of reservoirs showing different petrophysical characteristics is neglected by the geological genetic mechanism. (2) For engineering sweet spots, the evaluation of fracturing places a major focus on shale reservoirs, and it primarily starts from rock mechanics and other reservoir mechanical properties based on the effect of the brittleness index on fracturing.[26,27] For the tight conglomerate reservoir, its rock fabric characteristics differ from those of shale and have a complex hydraulic fracture propagation mechanism. Accordingly, the major controlling factors of fracturing of the tight conglomerate should be analyzed in depth. (3) In the evaluation method, after the geological and engineering sweet spot factors are optimized, the weight coefficients of various factors can be determined with the mathematical model to obtain the major controlling factors of productivity. However, according to the existing method, there has not been a clear standard for weight allocation. This makes the mathematical model difficult to interpret. The development effect of horizontal wells in the MA 131 small well spacing demonstration area has been varying significantly. The major controlling factors of high and stable production per well have been unknown, and there has been a rare comprehensive evaluation of the controlling factors of productivity. Thus, considering geological conditions and engineering design in the study area, it is urgent to build an evaluation system of the controlling factors of productivity of volumetric fractured horizontal wells for tight reservoirs. Therefore, an in-depth study was conducted on the existing problems and demands of tight oil reservoirs in the Baikouquan Formation of the MA 131 small well spacing demonstration area, Junggar Basin. The typical production dynamic model was divided comprehensively using geological, development, and engineering data. In this study, the random forest machine learning method was used to build an evaluation model of productivity controlling factors of the volume fractured horizontal wells in the tight reservoirs. This was done to provide a reference for production development and measure adjustment of tight oil reservoirs in the Baikouquan Formation, Junggar Basin.

2. GEOLOGICAL BACKGROUND

In general, the Triassic Baikouquan Formation in the MA 131 well block of Mahu Oilfield has a structural morphology of monocline with a southeast dip. Nose convex, groove, and platform structures have been developed locally and two groups of 10−40 m reverse faults have been developed in the study area.[28] From northeast to southwest, the MA 131 well block falls into three fault blocks: XIA 72 well fault block, MA 131 well fault block, and MA 133 well fault block (Figure 1a). As indicated by the data of conventional physical property by core analysis, the porosity of Baikouquan formation is 7.5−13.9%, thus an average of 8.84%. The permeability ranges from 0.03 to 17.20×10^{-3} mD, with an average of 0.96×10^{-3} mD. On the whole, the reservoir is characterized by high displacement pressure, poor pore structure, narrow capillary radius, micropore, and microfine throat. The crude oil from Baikouquan Formation is featured by prominent physical properties. It has a density of 0.8323 g/cm^3, a viscosity of 8.37 mPa·s, a coagulation point of 8.98 °C, and an initial distillation point of 130.96 °C.

Technical tests such as long horizontal section, dense cutting, small well spacing, large well cluster, and factory pattern have been performed for the design of a novel mode of production construction of domestic tight oil and ultralow permeability oil fields. This improves the single well production of EUR and increases drilling and completion engineering efficiency. Simultaneously, it effectively reduces

investment and cost, providing a foundation for scale efficiency construction. A high-efficiency stereo development demonstration area with a small well spacing was set near Well MA 15 in the middle of the MA 131 well block, that is, a rectangular area with a length of 1.9 km, a width of 0.79 km, and an area of 1.5 km^2 (Figure 1b). Oil layers of T_1b_2 and T_1b_3 are thick, and the ground conditions are simple. Thus, in this demonstration area, three-dimensional (3D) well pattern deployment can be performed since large platform implementation conditions are available.

The major development characteristics of the demonstration area are elucidated below. (1) In general, the reservoir driving type is elastic dissolved gas drive. (2) One set of well pattern was used for development. (3) There is rational development with natural energy. (4) In the form of well platform combinations, large well clusters were used to deploy wells. The well platform usually consisted of 4−6 wells. (5) The stimulation treatment of multistage and multicluster large-scale volume fracturing was used. Two development layers T_1b_3 and T_1b_{21} with a total of 12 wells were deployed in the demonstration area. T_1b_3 and T_1b_{21} have a well spacing of 100 and 150 m, respectively. In the deployment area, the geological reserves of T_1b_3 and T_1b_2 are about 5.15×10^6 and 2.42×10^6 bbl, respectively, making a total of 7.57×10^6 bbl. The design of single well production is about 235.2 bbl/d-249.9 bbl/d. The propping fracture exhibits a half-length of 70−90 m, a cluster spacing of 20 m, and a cross-seam spacing of 10 m. Thus far, all the 12 horizontal wells in the demonstration area have been put into production, yielding about 69.67×10^4 bbl of oil. Within the first 300 days after constructing the horizontal wells, the average daily oil production per well and the average accumulative oil production were 112.4 and 5.80×10^4 bbl, respectively.

For an accurate evaluation of the controlling factors of horizontal well productivity in the demonstration area, production dynamic modes should be separated in accordance with the production dynamic characteristics of the oil wells. The evaluation parameters indicating the production controlling factors should be improved. Subsequently, the classification criteria of the initial production level and the accumulated production level were set as listed in Table 1.

Table 1. Division Standard of Production Dynamic Mode

oil well type	daily oil production in the first 300 days (t/d)	cumulated oil production in the first 300 days (t)	representative well
I	>25	9000	MaHW1252
II	10−25	7500−9000	MaHW1242
III	<10	<7500	MaHW1243

This was done by considering the initial production level and accumulated production level of volume fractured horizontal wells in the tight reservoir (Table 2). Also, the two parameters average daily oil production and accumulated oil were considered in the first 300 days after fracturing fluid recovery. Under the set classification criteria, the production dynamic mode of horizontal wells in the study area was divided by integrating the initial production level and the accumulative production level. In the demonstration area, the typical production mode of the 12 horizontal wells is classified below. (1) Two horizontal wells with medium-high initial production and high cumulative production are classified as first-class oil wells (representing well MaHW1252). (2) Seven

horizontal wells with medium-high primary production and medium cumulative production decline are designated as Class II oil wells (corresponding to well MaHW1242). (3) Three horizontal wells with medium-high initial production and low cumulative production are classified as Class III oil wells (representing well MaHW1243).

3. METHODOLOGY

Machine learning algorithms have been extensively used in classification and regression problems. Many of these algorithms (e.g., Bayesian, logistic regression, support vector machine, decision tree, and so forth) are capable of solving classification problems. Compared with the existing three classification algorithms, the decision tree is easier to understand and has a mechanism that is simpler to explain.[29−31] The decision tree uses a top-down greedy algorithm to build a tree structure with an optimal attribute for splitting the respective internal node. The respective branch represents an attribute value. The tree is built recursively till the termination condition is satisfied. Each leaf node denotes the category of samples along this path. A considerable number of machine learning algorithms are black-box models, but their explainability is poor. However, through the visualization of the tree structure of the decision tree model, the classification rules of the model can be illustrated more effectively. The simple decision tree algorithm pertains to a single classifier showing bottlenecks in performance improvement and overfitting problems. Accordingly, an ensemble learning algorithm is proposed to improve prediction performance by integrating multiple classifiers. A random forest algorithm refers to an ensemble learning algorithm based on the decision tree, which builds an ensemble learning model with a decision tree as a base classifier.[32] According to Figure 2, this algorithm contains multiple decision trees that are trained using integrated learning techniques. The final classification result will be voted by the output result of all single decision trees when the samples to be classified are input. The implementation step of the algorithm is elucidated below.

1) Bootstrap (sampling scheme with replacement) is used to select N samples from the sample set as the training set.
2) A decision tree is built from the sample set obtained by sampling. Several d features are randomly and nonrepeatedly selected from the respective node, and the d features are used to divide the sample set to determine the best partitioning feature.
3) Steps 1 and 2 are repeated k times, with k denoting the number of decision trees in a random forest.
4) The trained random forest model is used to predict the test samples, and the voting method is used to indicate the predicted results.

The random forest algorithm is capable of detecting the interaction between features during the training process and then calculating their importance scores. During the evaluation of the feature importance of the random forest, Gini index GI can be the evaluation index, which is expressed as follows:

$$GI_m = 1 - \sum_{k=1}^{|K|} p_{mk}^2 \tag{1}$$

where K implies that there are K categories, and P_{mk} is the proportion of category K in node M.

Table 2. Statistics of Production in the Demonstration Area

| | present | | | | | | | | cumulated | | | | |
well	horizontal length(m)	oil nozzle (mm)	oil pressure (Mpa)	daily fluid (t)	daily oil (t)	daily gas (m³)	water cut (%)	gas oil ratio (m³/t)	cumulated fluid (t)	cumulated oil (t)	cumulated gas (10⁴ m³)	cumulated oil equivalent (t)	flow back rate (%)
MaHW1241	1791	5	11	25.6	12.1	69,522	52.7	5746	16335.8	9241.7	846	15983.2	19.1
MaHW1242	1802	4.5	11.2	31.1	20.9	19,720	32.8	944	13,722	7500.1	449	11074.8	12.2
MaHW1243	1802	4.5	6						12268.1	5354.2	211	7031.84	10.6
MaHW1244	1801	5	0.01						17991.1	7932.1	143	9073.36	18.3
MaHW1245	1765	4.5	3	23.4	10	3079	57.1	308	14301.9	5949.6	149	7133.49	21.3
MaHW1246	1802	4.5	13.5	40.2	26.9	57,782	33.1	2148	12761.7	7911.3	962	15580.4	16.8
MaHW1247	1803	5	18.8	3.9	3.9	49,598	1.1	12,717	10225.2	7127.5	564	11624.7	11.4
MaHW1248	1489	4	0.01	2	1.7		14.1		12865.7	8838.2	675	14217.5	16.7
MaHW1249	1606	4.5	9	30.5	13.4	23,068	56.1	1722	10650.3	6900.1	573	11462.9	15.6
MaHW1250	1600	4.5	9.2	37.1	26.5	41,780	28.7	1577	12717.9	8872.1	818	15388.3	12.6
MaHW1251	1622	4.5	9.8	30.1	18.6	45,078	38.2	2424	12244.1	8745.5	884	15789.2	10.6
MaHW1252	1780	5	14.8	25.9	19.3	40,808	25.6	2114	15398.5	10459.9	877	17445.3	20.5
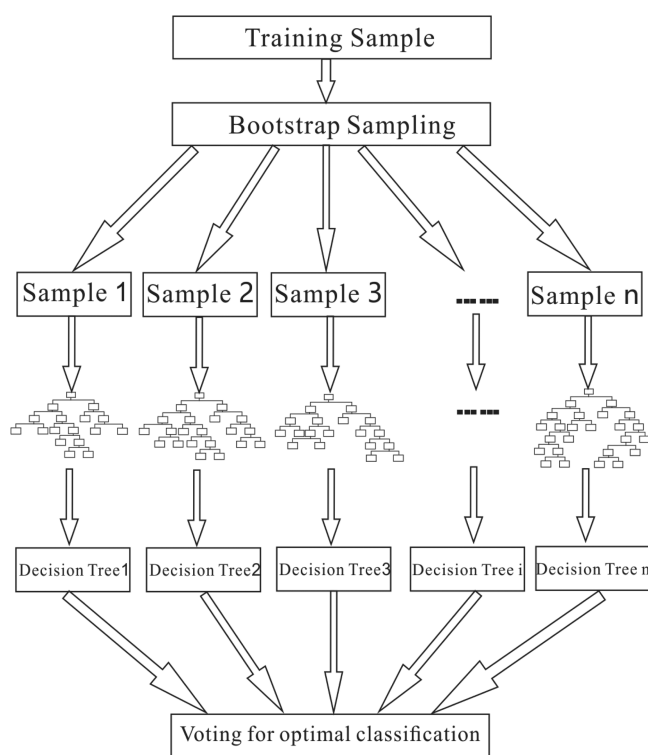
Figure 2. Schematic diagram of random forest algorithm.

Two samples are randomly selected from node M using different category markers. The variable importance score is expressed as VIM, and the Gini index score for the respective feature X_j is expressed as $VIM_j^{(\mathrm{Gini})}$. The importance of feature X_j in node M, that is, the Gini index change before and after branching in node M is written as

$$VIM_{jm}^{(\mathrm{Gini})} = GI_m - GI_l - GI_r \qquad (2)$$

where GI_l and GI_r are the Gini index of the two new nodes, respectively, after branching.

If the node in which feature X_j appears in the ith decision tree is set to M, the importance of X_j in the ith decision tree is expressed as follows:

$$VIM_{ij}^{(\mathrm{Gini})} = \sum_{m \in M} VIM_{jm}^{(\mathrm{Gini})} \qquad (3)$$

Assuming that there are k trees in the random forest, the importance of feature j is expressed as follows:

$$VIM_j^{(\mathrm{Gini})} = \sum_{i=1}^{k} VIM_{ij}^{(\mathrm{Gini})} \qquad (4)$$

4. OPTIMIZATION OF PRODUCTION FACTORS

4.1. Classification of Geological Sweet Spots Based on Petrophysical Facies. The geological sweet spot screening methods with the combination of various parameters reflecting reservoir quality on the plane have been generally used to determine the favorable area. In accordance with the research experience of geologists, appropriate evaluation parameters are selected to set classification evaluation standards. Although this method considers multiple parameters and obtains a quantitative reservoir classification scheme having significant physical properties and clear standards of reservoir quality classification, the major controlling factors of the formation of various reservoirs have not been determined. Meanwhile, the formation mechanism of geological dessert, which generally summarizes the classification of pure mathematical methods, is ignored. Research on the formation of dessert from the genetic mechanism and how to quantitatively characterize the reservoir quality variation between various reservoirs is limited. The concept of reservoir petrophysical facies was proposed by Professor Xiong Qihua in 1990 for reservoir classification and evaluation. This has been extensively used and developed.[33−35] Petrophysical facies can be defined as the genetic unit of the reservoir formed through a wide variety of geological processes, referring to the comprehensive effect arising from sedimentation, diagenesis, and later tectonic transformation. Petrophysical facies are capable of reflecting the macro and micropetrophysical attributes of the reservoir, as well as the geological genetic mechanism of different petrophysical characteristics. The favorable areas can be predicted according to the connotation of "geological facies" of petrophysical facies. The natural fractures in the study area are not developed, and the petrophysical facies are named primarily by sedimentation and diagenesis.
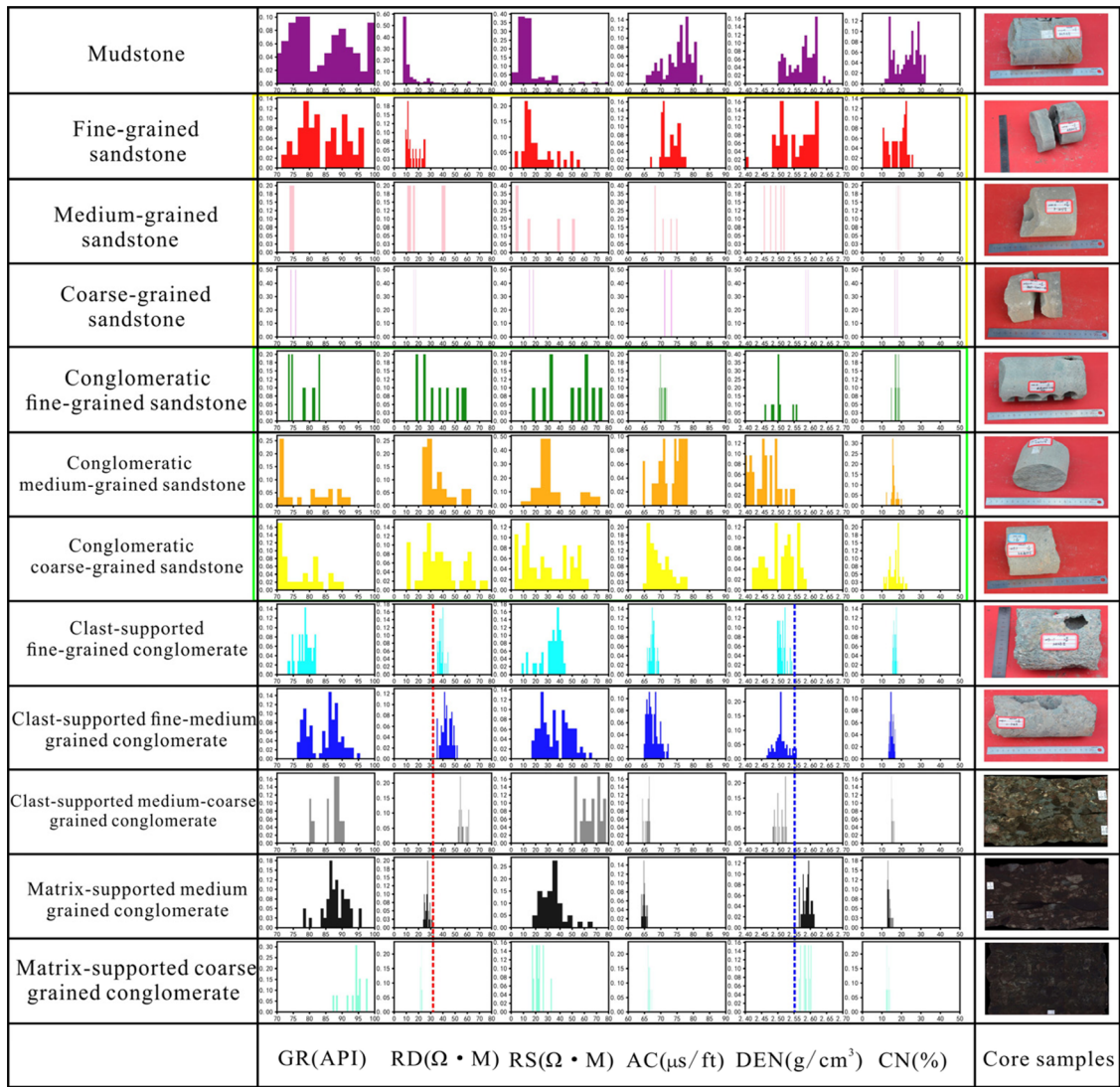
Figure 3. Cores and logging response characteristics of different lithofacies in the MA 131 well block.

4.1.1. Sedimentary Characteristics. The MA 131 well block is primarily made up of fan delta sedimentary systems with rapid accumulation near the source. Traction flow and gravity flow are the two sedimentary mechanisms in this block. The sedimentary thickness significantly changes in the vertical direction and the lithology changes rapidly. During the deposition of Baikouquan formation in the Mabei slope area, the tectonic activity was relatively weak with relatively flat terrain. Many river channels are featured with shallow cutting, fast migration, and violent swings. The conglomerate in the river channel is characterized by a variety of typical traction flow sedimentary structures (e.g., medium and large cross-bedding, imbricate gravel, as well as scouring surfaces). Moreover, the physical weathering of the parent rock produces numerous slope deposits with high density and high gravel content. This arises from the development of local paleotopographic slope breaks in the work area and the arid climate in the Early Triassic. Notably, the slope deposit and water are mixed to form block debris flow deposition characterized by high specific gravity, high gravel content, and high viscosity during the rainy season and flooding. On the whole, the content of gravel and sand in the debris flow sediment is high. The gravel in the sediment is higher than 30%, which is largely composed of sandy debris flow deposition. The typical characteristics are sophisticated particle sizes and poor sorting. Huge gravels can be found in sand-grade particles and matrices. The gravel is mainly filled with sandy-argillaceous sediments and is characterized by high argillaceous content, no bedding, as well as other sedimentary structures. The lithology of debris flow is predominantly composed of medium conglomerate with poor pore throat structures (Figure 3).

In the study area, the reservoir section of the Baikouquan formation has a large span of the rock particle size. The coarsest particles can contain coarse conglomerates with a particle size of 3−5 cm, and the finer can be of fine sandstone grade. The paleotopographic slope was relatively slow during the deposition of the Baikouquan formation. This led to a large coverage of the fan delta front accompanied by a far extension distance of the underwater distributary channel. Furthermore, among the interior of the same sedimentary microfacies, the grain size variation arising from sediment gravity differentiation also has a vital effect on the reservoir quality. As indicated by the core observation, the lithology of the Baikouquan formation reservoir section in the Mabei slope area covers sandy fine conglomerate, medium conglomerate, and gravelly (medium) coarse sandstone. In the same sedimentary
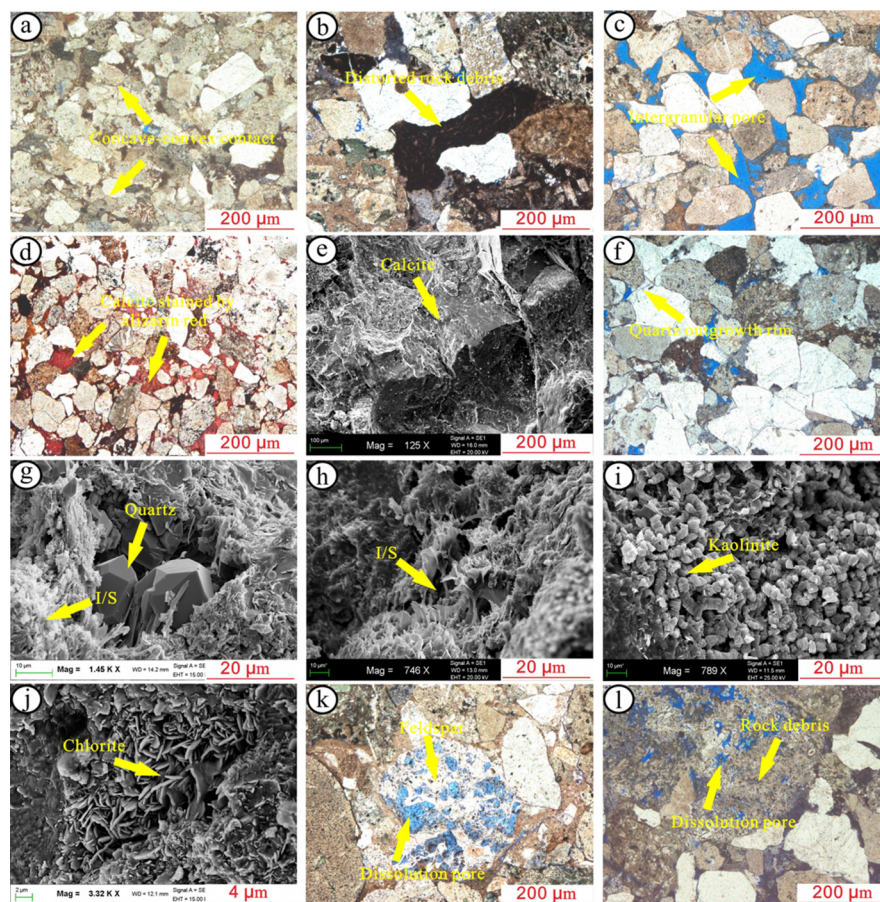
Figure 4. Major diagenetic characteristics of conglomerate-dominated reservoir: (a) Detrital particles exhibit concave-convex contacts (well XIA723, 2700.36 m, XPL). (b) Rock debris bending deformation (well MA154, 3006.53 m, XPL). (c) Residual intergranular pores (well MA139, 3258.11 m, XPL). (d) Crystalline calcite fills the intergranular pores, (well MA154, 3054.85 m, XPL). (e) Granulated crystal construction of calcite, (well MA13, 3107.29 m, SEM). (f) Quartz overgrowth (well XIA89, 2477.27 m, XPL) (g) Autogenous quartz attached to the I/S (well MA16, 3220.19 m, SEM). (h) Autogenous I/S fills the intergranular pores (well MA131, 3188.89 m, SEM). (i) Kaolinite occurs in a worm-shaped form (well MA132, 3261.37 m, SEM). (j) Leaf-shaped chlorite wraps the particle (well MA16, 3213.77 m, SEM). (k) Strong dissolution of feldspar particle (well MA154, 3051.83 m, XPL). (l) Dissolution of rock debris (well MA152, 3096.70 m, XPL).
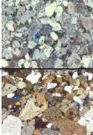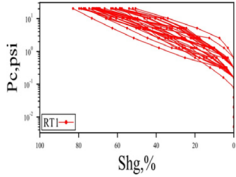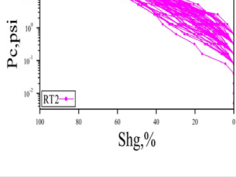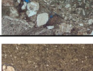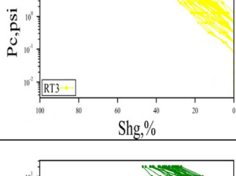
microfacies, the reservoir grain size is correlated with physical properties. Based on the comprehensive analysis of core, thin section, particle size, and mercury injection data, the reservoir quality can be ranked as gravelly (medium) coarse sandstone > fine conglomerate > medium conglomerate. The reservoir with a porosity of higher than 12% is mainly gravelly (medium) coarse sandstone while the reservoir with a porosity of less than 7% is dominated by medium conglomerate.

In this study, the division of lithofacies highlights the difference in the sedimentary mechanism while considering its significance in reservoir evaluation. Based on core observations, the corresponding relationship between the sedimentary mechanism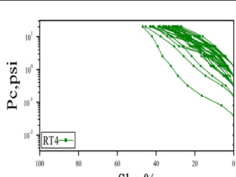 and lithofacies and the major controlling factors of reservoir physical properties was considered. With the sedimentary mechanism and the particle size as the boundary parameters, the conglomerate classification and naming standard (Q/SYXJ0195-2018) formulated by Xinjiang Oilfield was used to divide the lithofacies in the study area into four categories (i.e., mudstone, sandstone, matrix-supported conglomerate, and clast-supported conglomerate) and 12 subcategories. These include gravelly coarse sandstone, medium-fine sandstone, clast-supported fine conglomerate (particle size < 8 mm), and matrix-supported medium conglomerate (8 mm < particle size < 16 mm) (Figure 3). Logging facies were

thoroughly calibrated based on numerous core observations. As revealed by the analysis of logging responses of different lithofacies, GR, RD, and DEN logging curves have high identification effects on the lithofacies above. The DEN and RD show significant differences in conglomerate lithofacies with different particle sizes. For instance, sandy debris flow can be distinguished by high GR, high DEN, and low RD from other lithofacies.

4.1.2. Diagenetic Characteristics. Diagenetic facies are the product of a certain diagenesis and evolution stage of sediments under the action of diagenesis, fluid, and structure in a specific sedimentary and physicochemical environment. In accordance with the cast thin section and SEM observation in the study area, the reservoir has experienced strong compaction and the clastic particles are in line or in concave−convex contact (Figure 4a). Plastic rock debris is extruded and deformed (Figure 4b). As impacted by their strong anticompaction effect, mechanical compaction is restrained to a certain extent when quartz particles are in contact with one another. This allows the primary intergranular pores to be preserved (Figure 4c). There is common carbonate cementation with an average content of 6.45%, as indicated by XRD experimental analysis. The cement is chiefly calcite and iron calcite: the intergranular pores are

Table 3. Petrophysical Facies Characteristics and their Reservoir Quality Variation

reservoir type	petrophysical facies	lithofacies	diagenetic facies	pore type	thin section	mercury injection curve
I	PF1	fine-medium grained sandstone	weak compaction facies	intergranular pore		
	PF2	conglomeratic sandstone	weak compaction facies	intergranular pore		
	PF3	fine grained conglomerate	weak compaction facies	intergranular pore		
	PF5	fine-medium grained conglomerate	dissolution facies of unstable components	intragranular pore		
II	PF6	fine-medium grained conglomerate	weak compaction facies	intergranular pore		
	PF9	medium-coarse grained conglomerate	dissolution facies of unstable components	intragranular pore		
	PF10	medium-coarse grained conglomerate	weak compaction facies	intergranular pore		
III	PF4	fine grained conglomerate	cementation facies of clay minerals	micro pore; intercrystalline pore		
	PF7	fine-medium grained conglomerate	densification facies of compaction	micro pore		
IV	PF8	fine-medium grained conglomerate	cementation facies of calcite	intergranular pore		
	PF11	medium grained conglomerate (matrix supported)	densification facies of compaction	micro pore		
	PF12	coarse grained conglomerate (matrix supported)	densification facies of compaction	micro pore		

generally filled in the form of pore cementation in the late diagenetic stage (Figure 4d,e). There is low development of siliceous cement in the study area. This is because the reduction of primary pores is induced by the intensification of compaction by plastic rock debris. As a result, there is insufficient pore space for the precipitation of authigenic siliceous cement. Overgrowth of quartz (Figure 4f) and its idiomorphic prismatic crystals filling the pores were occasionally observed under the microscope (Figure 4g). The study of clay minerals is considered to be indispensable for diagenetic evolution analysis and diagenetic stage division. The dynamic changes in the diagenetic environment and fluid make it easy for clay minerals to transform from one another. On the whole, the clay minerals of the Baikouquan formation are composed of the illite-smectite mixed layer, kaolinite, and chlorite while montmorillonite has disappeared. The illite−smectite mixed layer is in honeycomb shape covering the surface of clastic particles (Figure 4h), thus plugging up the pore throat of the reservoir. Under acidic conditions, kaolinite is mainly filled in the intergranular pores as a worm shape (Figure 4i). Kaolinite is transformed into chlorite under the occurrence of iron and magnesium ions when the diagenetic environment turns into alkaline conditions. The above leaf-shaped chlorites have frequent existence along the rim of clastic particles in the form of pore-lining (Figure 4j), which contribute to the inhibition of the overgrowth of quartz and the protection of primary pores.

The dissolution of feldspar, volcanic debris, and other mineral components form secondary dissolution pores (Figure 4k.l). The dissolution of feldspar by organic acids is recognized as the most imperative dissolution of the Baikouquan formation reservoir.

As revealed by the above analysis of diagenesis, compaction, cementation, and dissolution are the major diagenesis affecting the reservoir quality of Baikouquan formation. The reservoirs have experienced early diagenetic stages A and B, most of which are at middle diagenetic stage A, while some deeply buried reservoirs are at middle diagenetic stage B. Compaction most severely impacts pore reduction, while dissolution is the most favorable diagenesis to improve reservoir quality. Following the major diagenetic characteristics and their influence on reservoir physical properties, the reservoir of Baikouquan formation can fall into five diagenetic facies. These are the two types of constructive diagenetic facies (i.e., weak compaction facies and dissolution facies of unstable components) and the three types of destructive diagenetic facies (i.e., cementation facies of clay minerals, cementation facies of calcite, and densification facies of compaction).

4.1.3. Reservoir Quality Variation. As indicated earlier, 12 lithofacies and 5 diagenetic facies were recorded in the fan delta of the Baikouquan formation. The petrophysical facies were determined primarily through sedimentation and diagenesis because of the nondevelopment of natural fractures in

the study area. The rational combination of lithofacies and diagenetic facies was performed to split the petrophysical facies into 12 types (Table 3). The mercury injection curve is capable of quantitatively characterizing the distribution of pore throat in porous media to determine the storage and flow capacity. Based on the construction and destruction of sedimentary facies and diagenetic facies, the mercury injection curves of 12 genetic petrophysical facies samples were clustered to categorize the reservoir quality. This was done to quantitatively characterize the reservoir quality variation between petrophysical facies of distinct origin. The clustering results characterized four types of reservoirs. PF1, PF2, PF3, and PF5 are characterized as type I reservoirs exhibiting relatively good physical properties. PF6, PF9, and PF10 are classified as type II reservoirs exhibiting medium physical properties. Type III and IV reservoirs exhibit poor physical properties (Table 3). All reservoir types show similar capillary pressure curve sets and pore throat radius distribution characteristics. From type I to type IV, their median pressure and displacement pressure increase continuously while their average pore throat radius decreases successively (Table 3), indicating the ceaseless deterioration of physical attributes and reservoir quality.

4.2. Optimization of Engineering Parameters. For tight conglomerate reservoirs largely produced by fracturing, whether fracturing can form a complex fracture network has an important effect on the producing degree of "fracture controlled" reserves and the high production of oil wells. There is insignificant difference in fracturing parameters (e.g., fracturing stage, interval spacing, cluster number, total sand concentration, total liquid volume, as well as sand-adding intensity). For the development of shale, the formation of a complex fracture network has a significant correlation with the brittleness index while conglomerate and shale exhibit completely different rock fabric characteristics. According to the uniqueness of tight conglomerate reservoir development, two important development theories (i.e., "fracture formation around gravel" and "active interference between wells") were proposed. Gravel content and gravel particle size, stress sensitivity, and brittleness were selected as engineering parameters to evaluate the complexity of the artificial fracture network.

4.2.1. Quantitative Characterization of the Gravel Content and Particle Size. The formation of a complex fracture network through reservoir fracturing requires favorable stress field conditions and rock fabric characteristics so that the fracture network can be further complicated under certain conditions by optimizing process technology. The reservoir in the demonstration area was featured by a large horizontal stress difference (higher than 10 MPa), undeveloped bedding fracture or natural fracture, and few brittle minerals, which have a negative effect on the formation of a complex fracture network. As indicated by numerous coring and triaxial hydraulic fracturing simulations, the fracture propagates primarily around gravel, occasionally through the gravel, and terminates when encountering gravel. According to the difference in rock fabric between coarse-grained sedimentary conglomerate and fine-grained sedimentary shale, it is found that they have completely different mechanical properties and fracture forming mechanisms. In general, the hydraulic fracture is formed and extended along the gravel edge on the weak cementation surface between gravel and the matrix. Gravel penetrating fractures can be formed when the dissolution of conglomerate is strong, when there are numerous dissolution

pores, or when there is calcite cementation. The strong heterogeneity due to the change in the gravel particle size and the gravel content can significantly control the formation of a complex fracture network. As revealed by the numerical simulation of the fracture propagation process, the fracture continues to bifurcate and complicate during the fracture propagation process under the combined effect of tension and shear force. Conglomerates with different gravel contents and particle sizes have completely different fracture propagation laws. The higher the content of gravel, the more the branch fractures and the higher the tortuosity and bandwidth of the fractures.

According to the above analysis, how to quantitatively characterize the gravel particle size and gravel content is the key factor in the formation of a complex fracture network. The petrophysical analysis of different lithofacies calibrated by logging demonstrates a significant positive correlation between the gravel particle size and resistivity. However, the gravel content and the gravel particle size are difficult to quantitatively characterize. The gravels are bright white on the formation microscanner image (FMI) image because of their high resistivity characteristics. Their development is analyzed using numerous FMI images. The gravels with different particle sizes and contents are extracted to establish the quantitative gravel content and particle size logging interpretation model using computer vision technology. The specific implementation steps are detailed below (Figure 5).
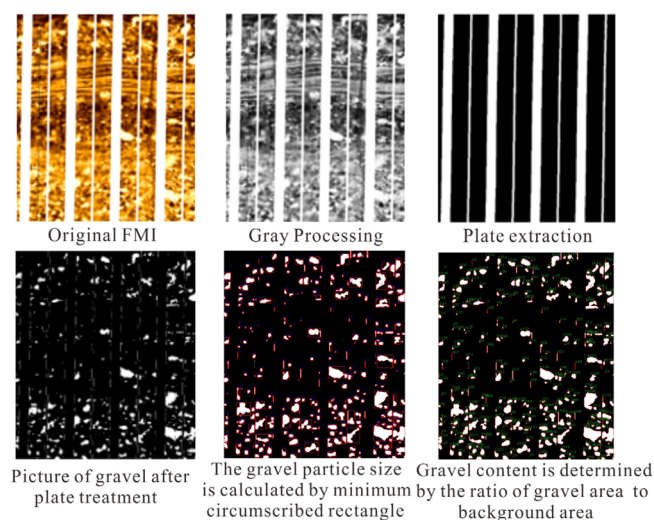

Figure 5. FMI processed by computer vision technology.

(1) Greyscale processing of the FMI image. (2) Processing the plate of imaging logging photographs in accordance with the color gamut. (3) Determining the gravel particle size by the minimum circumscribed rectangular diagonal length of gravel. (4) Determining the gravel content by the ratio of gravel to the background pixel value. According to the quantitative interpretation of the FMI gravel particle size and content, the conventional well logging is calibrated, and the interpretation model of single well gravel particle size and content is built (Figure 6). The interpretation results are consistent with the original FMI image.

4.2.2. Stress Sensitivity. The reservoir is quite dense, and the horizontal stress difference is high. This causes the failure of fracturing due to nonpenetration of oil pay or high pump pressure. The difference in horizontal stress determines the
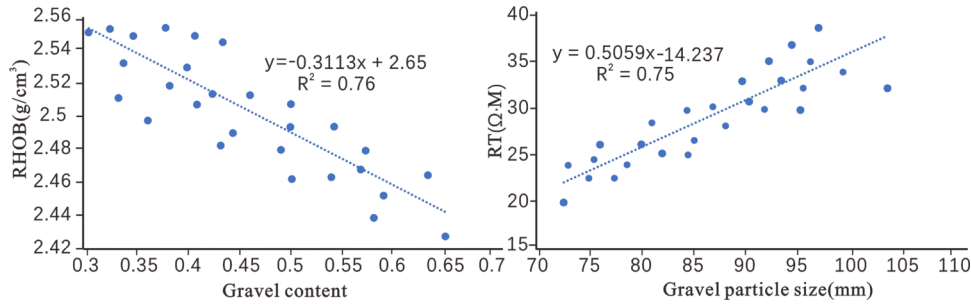
Figure 6. Logging interpretation model of the gravel content and the gravel particle size.
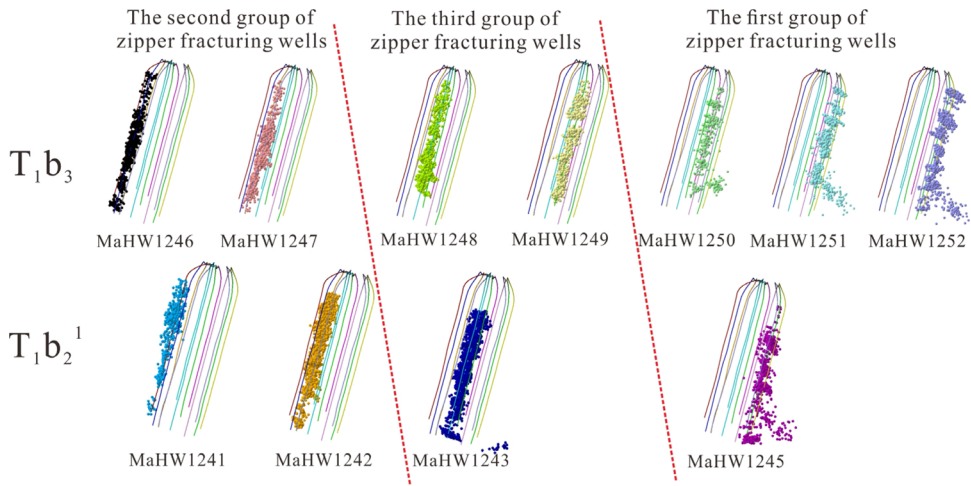

Figure 7. Microseismic monitoring results of horizontal wells in the demonstration area.

Table 4. Microseismic Monitoring Parameters of Horizontal Wells in the Demonstration Area

fracturing order	formation	well	average closure pressure (MPa)	SRV (m³)	average aspect ratio of artificial fracture	average fracture height (m)	number of microseismic events
the first group of fracturing wells	$T_1b_2^1$	MaHW1245	22.6	198	3.1	41.8	1265
	T_1b_3	MaHW1250	23.2	125	5.1	36.0	811
		MaHW1251	23.6	173	3.2	36.7	1420
		MaHW1252	21.7	162	4.1	29.7	1452
the second group of fracturing wells	$T_1b_2^1$	MaHW1241	24.2	218	2.8	26.1	575
		MaHW1242	26.3	245	2.7	27.6	1296
	T_1b_3	MaHW1246	24.8	152	2.4	24.5	1091
		MaHW1247	25.7	168	2.7	26.0	1032
the third group of fracturing wells	$T_1b_2^1$	MaHW1243	30.8	252	2.2	28.4	1648
	T_1b_3	MaHW1248	27.1	183	2.2	29.0	1071
		MaHW1249	28.9	185	2.1	28.2	1112

difficulty of opening and propagation of artificial fractures, and the maximum horizontal stress determines the propagation direction of artificial fractures. Thus, the premise of successful fracturing of the complex tight reservoir is to master the characteristics and laws of in situ stress. The hydraulic fracturing of large well-spacing horizontal wells in the Mahu conglomerate reservoir reveals that the artificial fractures are mainly two wing fractures with simple fracture network structure. The difficulty to form a complex fracture network causes insufficient reserve production. The hydraulic fracture is easy to expand along the direction of the maximum horizontal stress. The high horizontal stress difference limits the deflection distance of the fracture and makes it easy to form a narrow and long fault zone. Furthermore, the propagation path of hydraulic fracture is relatively random under low horizontal stress differences. Fracture bifurcation can improve the complexity of the fracture network. After the dense cutting measures are taken, the stress interference is enhanced. The spatial stress field under the effect arising from the inter-well interference leads to the change in the original in-situ stress state and the reduction of stress difference around the wellbore. This facilitates the formation of artificial fractures. On that basis, the fracture network is connected and the reservoir reconstruction volume increases. One set of well patterns and stereo staggered well arrangement are combined to form the active utilization technology of the spatial stress field to maximize the beneficial interference from the plane and vertical view.

The field application also reveals the effectiveness of the active utilization technology of the spatial stress field. The small well spacing and fine perforation clustering of zipper fractured by one set of well pattern cause considerable filling in

Table 5. Comparison between the Measured Rock Mechanical Parameters and the Calculated Values

| well	formation	coring depth (m)	Young's modulus (GPa)			Poisson ratio		
			measured value	calculated value	precision (%)	measured value	calculated value	precision (%)
MA133	$T_1b_2^1$	3300	27.4	27.9	98	0.19	0.23	80
MA139	T_1b_3	3288.34	27.43	29.1	94	0.194	0.23	81
MA154	T_1b_3	3019.01	23.69	24	98	0.185	0.2	92
MA139	$T_1b_2^1$	3294.87	27.18	24.2	90	0.188	0.21	88
MA137	$T_1b_2^1$	3262.83	27.99	26.1	93	0.207	0.18	87
MA154	$T_1b_2^1$	3054.02	22.79	24.5	92	0.249	0.22	89
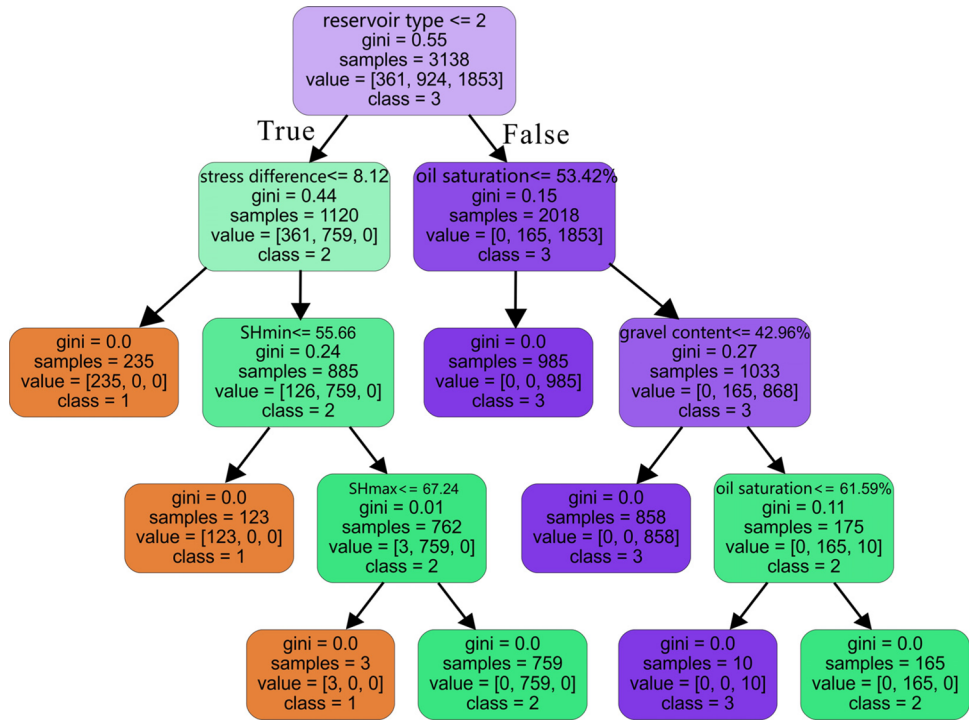
Figure 8. Visualization of one decision tree of the random forest algorithm.

the direction of the minimum horizontal stress. This increases the minimum horizontal stress (the DFIT of two wells shows an increase of 10%) and decreases the horizontal stress difference. According to the microseismic monitoring data, the stress interference makes the fracture network more complex (Figure 7). The SRV (reservoir reconstruction volume) of the postfracturing wells is larger while the aspect ratio is smaller (Table 4). The computation method of horizontal in-situ stress proposed by Huang is employed in this study.[36] The minimum horizontal stress of the postfractured wells changes because of the positive intervention of the stress field. Thus, the calculated results are corrected to approximate closure pressure.

4.2.3. Brittleness Index. Complex fractures are more likely to form when a large number of brittle minerals are present in a reservoir during fracturing. This can lower the burst pressure, enhance the conductivity of artificial fractures, and fully reform the reservoir. Young's modulus and Poisson ratio are two basic rock mechanical parameters reflecting rock brittleness. Young's modulus ascertains the ability of the reservoir to resist deformation whilst the Poisson ratio determines the ability of the reservoir to attain transverse deformation after stress. The higher Young's modulus, the lower the Poisson ratio and the stronger the brittleness.

The corresponding logging interpretation model of rock mechanical parameters was built to obtain the rock mechanical

properties of the reservoir section. For conglomerate reservoirs, the plasticity increases with an increase in the composition of andesitic and basaltic tuff whilst the brittleness increase with an increase in the composition of granite. This implies that a rock mechanics parameter interpretation model should be built for the conglomerate reservoir of the Baikouquan formation in the Mahu sag. S-wave slowness indicates the characteristics of formation compression and shear resistance, which are the basic data for calculating Young's modulus and the Poisson ratio. However, most conventional well logging only measures P-wave slowness. The logging data of key exploration wells with measured S-wave slowness logging were selected to regress the P-wave slowness conversion relationship. This is to determine the rock mechanics parameters of the respective single well reservoir section in accordance with the regression relationship. The relative error between the obtained rock mechanical parameters and the rock mechanical parameters measured in the test is less than 5% (Table 5). This confirms that the calculation results are accurate and reliable. The prediction of one-dimensional rock mechanical parameters has higher accuracy (Young's modulus > 90%, Poisson ratio > 80%).

5. RESULTS AND DISCUSSION

A total of 3138 data samples are input into the random forest model using the classification of the oil well production performance model as the label and reservoir type, oil saturation, horizontal stress difference, minimum horizontal stress, gravel content, gravel particle size, and brittleness as the features. In the random forest model, each decision tree is composed of internal nodes representing features or attributes and leaf nodes representing categories. The respective branch of the tree represents a possible decision result, and each path from the root node to different leaf nodes in the decision tree suggests a decision rule. Thus, the respective decision tree can be considered as a series of linearized decision rules. The decision-making process of the model is explained by visualizing a decision tree in a random forest. As illustrated in Figure 8, each node contains information such as variable name, Gini index, sample number, and corresponding classification category. The root node of this decision tree is divided following the value of the reservoir type. Those with a value of less than or equal to 2 (true) are assigned to the left. Those with a value greater than 2 (false) are assigned to the right. The Gini index division standard of each node is determined by calculating the Gini index of multiple variables. The variable that achieves the largest Gini index is considered the division feature. The maximum Gini index in this root node is 0.55 and its corresponding variable is the reservoir type with the division value of 2. The division result of root node samples implies that 361 samples (11.5%) are grouped in class 1, 924 samples (29.4%) in class 2, and 1853 samples (59.1%) in class 3. Samples (1120) with a petrophysical facies value of less than or equal to 2 (true) are grouped into the second layer subnode on the left. The remaining 2018 samples with a petrophysical facies value greater than 2 are grouped into the second layer subnode on the right. According to this rule, the above samples branch down the decision tree by calculating the Gini index of all variables until its calculation result is 0. The decision tree in Figure 8 reveals that the reservoir type, horizontal stress difference, and oil saturation are the major characteristics for determining the category of oil wells.

We use a massive data set consisting of 3138 samples from 13 boreholes from a deeply buried deposit in the Junggar Basin, Western China. To do this, we selected the feature from two aspects: petrophysical facies that are capable of indicating the genetic mechanism of geological dessert and engineering dessert parameters forming complex fracture networks. We then trained our RF model on 80% of the data to predict the oil well class using the selected features as primary inputs. Table 6 shows the parameters requiring adjustment of the RF model and corresponding optimal parameters. We evaluated the machine learning method on the remaining 20% of the data to test the model performance. The results indicated that the RF model produced excellent results with only 12

misclassifications across the entire data set of 627 samples, which represent <2% error. In order to statistically test the significant difference regarding the predictive accuracy of the RF model, we applied the chi-square test. The same conclusion is reinforced by the chi-square test results. The test is statistically significant under 99% confidence level.

During the calculation of random forest based on multiple trees, the importance of each feature can be obtained according to the average reduction of the Gini index in all nodes. The model calculates the importance of the respective feature to the oil well category (Figure 9), in which the reservoir type, oil
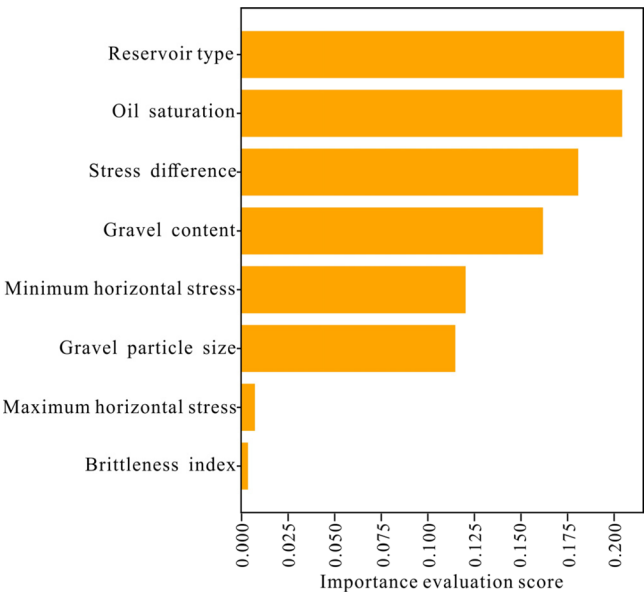

Figure 9. Importance of the evaluation score of each feature in the random forest algorithm.

saturation, horizontal stress difference, and gravel content are the most important four indicators, with each value exceeding 15%. Brittleness and maximum horizontal stress are considered the least important indexes, with values of less than 5%, indicating that they have limited impact on determining oil well types. The cumulative importance of the first four indicators accounts for 81.78%, implying that these indicators play a decisive role in the final oil well productivity. The important variables predicted by random forest demonstrate that excellent reservoir type and high oil saturation are the material foundation for high and stable production of oil wells. Stress difference and gravel content are the key factors that determine the formation of a complex fracture network.

Until now, there have been enormous applications by employing random forest to solve classification and regression tasks. Gordon et al. evaluated the use of a random forest and machine learning(ML) model to predict HI and OI from four wells from the offshore east coast of Newfoundland, Canada.[37] The model was evaluated using the mean absolute error (MAE), root mean square error (RMSE), correlation of determination (R^2), and Spearman's rank correlation (R^2). Tiwary et al. developed an RF-based model to classify different phases of coal macerals (organic constituents) and minerals (inorganic constituents).[38] A comparative analysis suggested that the final output shows better than 90% classification accuracy compared to ground truth. Maxwell proposed a quantile regression forest algorithm as an alternative method to

Table 6. Critical Hyperparameters and Optimal Parameter Values for the RF Model

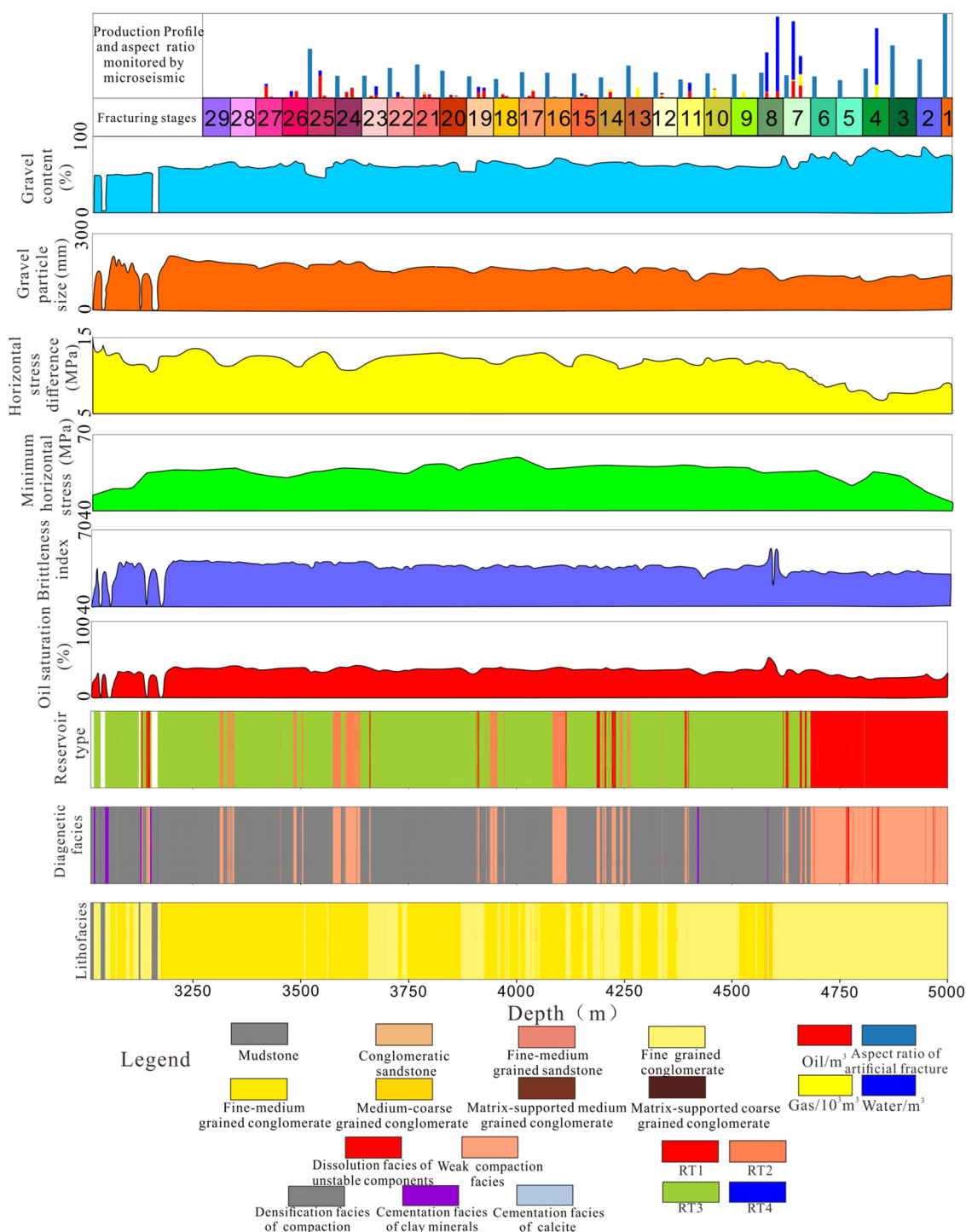| classification model	optimized parameter	search range	optimal parameter
RF	number of estimators	1−100	58
	learning rate	0.01−1	0.26
	min_samples_split	2−8	5
	maximum depth of the tree	1−20	8

Figure 10. Diagram of the production profile, the aspect ratio of the microseismic fracture, and various geological and engineering parameters of well MaHW1243.

spatially model coal properties.[39] Other examples based on RF include predicting coal wettability for CO_2 sequestration purpose,[40] identifying altered and nonaltered lithotypes,[41] solar power forecast,[42] forecasting accuracy of daily enterprise electricity consumption,[43] and so forth. However, the aforementioned approaches primarily concentrate on data preprocessing, feature selection, hyperparameter optimizing, and model performance. It has been rarely focused on visualizing the trees to understand and analyze the sensitivity and importance of the selected feature evaluated in this study.

Well MaHW 1243 measured by FSI (flow scanning imager) was selected to obtain the oil, gas, and water production profile of the respective fracturing section through comprehensive interpretation. This was done to verify the rationality of feature importance analysis. Subsequently, the productivity controlling factors were analyzed by comparing the production profile with the geological and engineering parameters of each fracturing section. The horizontal section of the well is divided into 29 sections according to their respective hydraulic fracturing. The liquid production is mainly derived from the fracturing sections

1−14. In general, the lithofacies of these sections are composed of fine conglomerate while the diagenetic facies largely consist of weak compaction facies which correspond to type I reservoir quality. However, it mainly produces water due to low oil saturation. On the whole, the horizontal well is well fractured, and the fracture aspect ratio is low. The horizontal stress difference in the 2nd−6th fracturing section and the aspect ratio of the fracture network monitored by microseismic is small, which reveals that a complex fracture network system has been formed. Fracturing sections 1−3, 6, 7, 9, 10, and 11 are the major oil-producing layers of which oil production accounts for 85.80% of the total oil production. Although they correspond to good saturation, reservoir type III is largely developed, and the thickness of reservoir type II is relatively small. Water production is primarily derived from the well section below 4535 m. Impacted by the development of reservoir type III in the postfracturing section, the production is pretty low ([Figure 10](#)). Furthermore, the reservoir type and oil saturation are the major factors affecting oil well productivity based on the formation of a complex fracture network as a whole.

6. CONCLUSIONS

With the tight conglomerate reservoir in the MA 131 well block as the research area, the volume fractured small well spacing horizontal wells in the demonstration area are divided into three dynamic production modes according to the initial and cumulative production level. The factors of the productivity of horizontal wells in the demonstration area were analyzed in terms of geology and engineering.

Furthermore, the sedimentary characteristics and diagenesis in the study area were analyzed in accordance with the coring, cast thin section, and SEM data. The reservoirs are divided into 12 lithofacies types and five diagenetic facies types. Given the formation mechanism of the geological sweet spot, 12 petrophysical facies were identified by combining lithofacies and diagenetic facies. The mercury injection curves were clustered to quantitatively characterize the reservoir quality variation between reservoirs of different origins: the results proved four reservoir types. According to the uniqueness of tight conglomerate development, three aspects of gravel content and gravel particle size, stress sensitivity, and brittleness were used as the engineering parameters to evaluate the complexity of an artificial fracture network. Computer vision technology was used to build the quantitative logging interpretation model of the gravel content and the gravel particle size. The calculated minimum horizontal stress was corrected using the closure pressure, and the empirical regression formula was used to calculate the rock mechanics parameters. The calculation results are accurate and reliable, which can act as the feature input of the random forest algorithm.

The random forest model was built to analyze the effect of different features on oil well categories and the importance of the respective feature in the classification process. This is done by using the oil well production mode as the label and different optimized geological and engineering parameters as the features. The results indicated that the RF model produced excellent results with only 12 misclassifications across the entire data set of 627 samples, which represent <2% error. As indicated by the evaluation result, the reservoir type, oil saturation, horizontal stress difference, and gravel content are the most important four indicators, with each value exceeding

15%. Brittleness and maximum horizontal stress are considered the least important indexes, with values of less than 5%. Reservoir quality and oil saturation are the material foundation for oil wells' high and stable production. Moreover, stress difference acts as the major controlling factor in the formation of a complex fracture network, followed by gravel content. The research results of this study clarify the major controlling factors of oil well productivity from the perspective of geology and engineering, which lay a theoretical foundation for the site selection of small well-spacing 3D development platforms and the optimization of horizontal well deployment in the future. To our knowledge, this is the first time that an RF approach has been used to classify the oil wells. The results of this paper have proved the great potential of the ML method in the petroleum field. However, the current model has limitations in the following aspects: (1) There is a lack of experimental validation of the results presented. (2) The applicability of the current RF model has not been fully understood. Although the model has been trained with the data, it is unclear whether new data can be adopted or if it can act as a pretrained model for other different working scenarios. It is highly recommended that the future study focuses on making black-box machine learning models more transparent, thus making them interpretable and easily understood.

■ AUTHOR INFORMATION

Corresponding Author
Zhizhang Wang − *College of Geosciences, China University of Petroleum, Beijing 102249, China*; Email: wang_zhizhang@126.com

Authors
Zhichao Yu − *College of Geosciences, China University of Petroleum, Beijing 102249, China*; ⓞ orcid.org/0000-0002-9583-8521
Qingping Jiang − *Xinjiang Oilfield Company Research Institute of Exploration & Exploitation, Karamay, Xinjiang 834000, China*
Jie Wang − *CNOOC China Limited, Shenzhen Branch, Shenzhen, Guangdong 518064, China*
Jingrong Zheng − *College of Geosciences, China University of Petroleum, Beijing 102249, China*
Tianyou Zhang − *CNOOC Research Institute Co., Ltd., Beijing 100028, China*

Complete contact information is available at:
https://pubs.acs.org/10.1021/acsomega.2c02546

Author Contributions
Z. Y.: writing—original draft, methodology, software, writing—review and editing. Z. W.: project administration and supervision. Q. J.: resources and supervision. J. W.: data curation and editing. J. Z.: formal analysis. T. Z.: Editing.

Notes
The authors declare no competing financial interest.

their thorough and critical suggestions, which have significantly helped improve the quality of this paper.

■ REFERENCES

(1) Er, C.; Zhao, J.; Li, Y. Relationship between tight reservoir diagenesis and hydrocarbon accumulation: An example from the early Cretaceous Fuyu reservoir in the Daqing oil field, Songliao Basin, China. *J. Pet. Sci. Eng.* **2022**, *208*, No. 109422.

(2) Yan, S.; Qun, L. U. O.; Jiang, Z. Enrichment of tight oil and its controlling factors in central and western China. *Pet. Explor. Dev.* **2021**, *48*, 492−506.

(3) Longde, S.; Caineng, Z.; Ailin, J. Development characteristics and orientation of tight oil and gas in China. *Pet. Explor. Dev.* **2019**, *46*, 1073−1087.

(4) Zhao, W. B.; Hu, S. Y.; Deng, X. Q. Physical property and hydrocarbon enrichment characteristics of tight oil reservoir in Chang 7 division of Yanchang Formation, Xin'anbian oilfield, Ordos Basin, China. *Pet. Sci.* **2021**, *18*, 1294−1304.

(5) Nengwu, Z.; Shuangfang, L. U.; Min, W. Limits and grading evaluation criteria of tight oil reservoirs in typical continental basins of China. *Pet. Explor. Dev.* **2021**, *48*, 1089−1100.

(6) Tariq, Z.; Mahmoud, M.; Alade, O.; Abdulraheem, A.; Mustafa, A.; Mokheimer, E. M. A.; Al-Jawad, M.; Al-Nakhli, A. Productivity Enhancement in Multilayered Unconventional Rocks Using Thermochemicals. *ASME. J. Energy Resour. Technol.* **2021**, *143*, No. 033001.

(7) Tariq, Z.; Mahmoud, M.; Abdulraheem, A.; Al-Shehri, D.; Murtaza, M. An Environment Friendly Approach to Reduce the Breakdown Pressure of High Strength Unconventional Rocks by Cyclic Hydraulic Fracturing. *ASME. J. Energy Resour. Technol.* **2020**, *142*, No. 043002.

(8) Tariq, Z.; Mahmoud, M.; Abdulraheem, A.; Al-Nakhli, A.; BaTaweel, M. An experimental study to reduce the breakdown pressure of the unconventional carbonate rock by cyclic injection of thermochemical fluids. *J. Pet. Sci. Eng.* **2020**, *187*, No. 106859.

(9) Mustafa, A.; Tariq, Z.; Abdulazeez Abdulraheem, M. M. et al. Shale Brittleness Prediction using Machine Learning−A Middle East Basin Case Study 2. *AAPG Bull.* **2022** 20,220,110.

(10) Tariq, Z.; Hassan, A.; Al-Abdrabalnabi, R.; et al. Comparative Study of Fracture Conductivity in Various Carbonate Rocks Treated with GLDA Chelating Agent and HCl Acid. *Energy Fuels* **2021**, *35*, 19641−19654.

(11) Al-Nakhli, A.; Tariq, Z.; Mahmoud, M. Thermochemical-Pulse Fracturing of Tight Gas: Investigation of Pulse Loading on Fracturing Behavior. In *SPE Middle East Oil & Gas Show and Conference*; OnePetro, 2021.

(12) Kalam, S.; Afagwu, C.; Al, J. J. A review on non-aqueous fracturing techniques in unconventional reservoirs. *J. Nat. Gas Sci. Eng.* **2021**, *95*, No. 104223.

(13) Tariq, Z.; Aljawad, M. S.; Murtaza, M.; Mahmoud, M.; Al-Shehri, D.; Abdulraheem, A. A Data-Driven Approach to Predict the Breakdown Pressure of the Tight and Unconventional Formation. In *Paper presented at the SPE Annual Technical Conference and Exhibition, Dubai, UAE*, September 2021.

(14) Xiaojun, W.; Yong, S.; Menglin, Z. Composite petroleum system and multi-stage hydrocarbon accumulation in Junggar Basin. *China Pet. Explor.* **2021**, *26*, 29−43.

(15) Lei, D.; Li, X.; Wanxiang, Y. Establishment and Application of the Optimized Evaluation System for Seismic Exploration in Junggar Basin. *Xinjiang Pet. Geol.* **2021**, *42*, 720−725.

(16) Jun, L. I.; Yong, T.; Tao, W. U. Overpressure origin and its effects on petroleum accumulation in the conglomerate oil province in Mahu Sag, Junggar Basin, NW China. *Pet. Explor. Dev.* **2020**, *47*, 726−739.

(17) Aydin, G, Kaya, S, Karakurt, I. Modeling of coal consumption in Turkey: An application of trend analysis. In *24th International Mining Congress and Exhibition of Turkey, Antalya, Turkey*, 2015, pp. 83−87.

(18) Aydin, G. Regression models for forecasting global oil production. *Pet. Sci. Technol.* **2015**, *33*, 1822−1828.

(19) Wu, W.; Li, Q.; Pei, J. Seismic sedimentology, facies analyses, and high-quality reservoir predictions in fan deltas: A case study of the Triassic Baikouquan Formation on the western slope of the Mahu Sag in China's Junggar Basin. *Mar. Pet. Geol.* **2020**, *120*, No. 104546.

(20) Xi, K.; Cao, Y.; Haile, B. G. Diagenetic variations with respect to sediment composition and paleo-fluids evolution in conglomerate reservoirs: A case study of the Triassic Baikouquan Formation in Mahu Sag, Junggar Basin, Northwestern China. *J. Pet. Sci. Eng.* **2021**, *197*, No. 107943.

(21) Xiao, Z.; Chen, S.; Liu, C. Lake basin evolution from early to Middle Permian and origin of Triassic Baikouquan oil in the western margin of Mahu Sag, Junggar Basin, China: Evidence from geochemistry. *J. Pet. Sci. Eng.* **2021**, *203*, No. 108612.

(22) Jianjun, C.; Dingwei, W. CNPC's progress in horizontal well fracturing technologies for unconventional reservoirs. *Nat. Gas Ind.* **2017**, *37*, 79−84.

(23) Jianhua, Q.; Jing, Z.; Qingping, J. Sweet spot classifi cation evaluation of tight conglomerate reservoir in Mahu sag and its engineering application. *China Pet. Explor.* **2020**, *25*, 110−119.

(24) Zou, Y.; Shi, S.; Zhang, S. Experimental modeling of sanding fracturing and conductivity of propped fractures in conglomerate: A case study of tight conglomerate of Mahu sag in Junggar Basin, NW China. *Pet. Explor. Dev.* **2021**, *48*, 1383−1392.

(25) Li, G.; Qin, J.; Xian, C.; Fan, X.; Zhang, J.; Ding, Y. Theoretical understandings, key technologies and practices of tight conglomerate oilfield efficient development: A case study of the Mahu oilfield, Junggar Basin, NW China. *Pet. Explor. Dev.* **2020**, *47*, 1185−1197.

(26) Shaibu, R.; Guo, B.; Wortman, P. B. Stress-sensitivity of fracture conductivity of Tuscaloosa Marine Shale cores. *J. Pet. Sci. Eng.* **2022**, *210*, No. 110042.

(27) Han Cao, Y.; Zhao, Q. G.; Bao, T.; Sun, P. An insight into shale's time-dependent brittleness based on the dynamic mechanical characteristics induced by fracturing fluid invasion. *J. Nat. Gas Sci. Eng.* **2021**, *96*, No. 104312.

(28) Jiangwen, X.; Li Jianmin, W.; Yuanyue, D. K.; Hong, J. Exploration and practice of volume fracturing technology in horizontal well of Mahu tight conglomerate reservoirs. *China Pet. Explor.* **2019**, *24*, 241−249.

(29) Wang, Y.; Xia, S. T. Unifying attribute splitting criteria of decision trees by Tsallis entropy. In *Acoustics Speech and Signal Processing, IEEE International Conference*, 2017, pp. 2507−2511.

(30) Ren, Q.; Zhang, H.; Zhang, D.; Zhao, X.; Yan, L.; Rui, J. A novel hybrid method of lithology identification based on k-means++ algorithm and fuzzy decision tree. *J. Pet. Sci. Eng.* **2022**, *208*, No. 109681.

(31) Yu, Z.; Wang, Z.; Zeng, F. Volcanic lithology identification based on parameter-optimized GBDT algorithm: A case study in the Jilin Oilfield, Songliao Basin, NE China. *J. Appl. Geophys.* **2021**, *194*, No. 104443.

(32) Acharjee, A.; Kloosterman, B.; Visser, R. G.; Maliepaard, C. Integration of multi-omics data for prediction of phenotypic traits using random forest. *BMC Bioinform.* **2016**, *17 Suppl 5*, 180.

(33) Qihua, X.; Shimi, P.; Shuwang, H. A preliminary study of the new concept of petrophysical facies and its initial application in Lengdong-Leijia region in Liaohe Depression. *Acta Pet. Sin.* **1994**, *15*, 69−75.

(34) Xiong, Q, Wang, Z. *Modern reservoir geology, theory and technology*; Petroleum Industry Press: Beijing, 2010; pp. 63−70.

(35) Jin, L.; Guiwen, W.; Min, C. Pore structures evaluation of low permeability clastic reservoirs based on petrophysical facies: A case study on Chang 8 reservoir in the Jiyuan region, Ordos Basin. *Pet. Explor. Dev.* **2013**, *40*, 606−614.

(36) Huang, R.; Zhuang, J. A new prediction method of formation fracture pressure. *Pet. Drill. Prod. Technol.* **1986**, *3*, 1−14.

(37) Gordon, J. B.; Sanei, H.; Pedersen, P. K. Predicting hydrogen and oxygen indices (HI, OI) from conventional well logs using a Random Forest machine learning algorithm. *Int. J. Coal Geol.* **2022**, *249*, No. 103903.

(38) Tiwary, A. K.; Ghosh, S.; Singh, R. Automated coal petrography using random forest. *Int. J. Coal Geol.* **2020**, *232*, No. 103629.

(39) Maxwell, K.; Rajabi, M.; Esterle, J. Spatial interpolation of coal properties using geographic quantile regression forest. *Int. J. Coal Geol.* **2021**, *248*, No. 103869.

(40) Ibrahim, A. F. Application of various machine learning techniques in predicting coal wettability for CO_2 sequestration purpose. *Int. J. Coal Geol.* **2022**, *252*, No. 103951.

(41) Maxwell, K.; Rajabi, M.; Esterle, J. Automated classification of metamorphosed coal from geophysical log data using supervised machine learning techniques. *Int. J. Coal Geol.* **2019**, *214*, No. 103284.

(42) Liu, D.; Sun, K. Random forest solar power forecast based on classification optimization. *Energy* **2019**, *187*, No. 115940.

(43) Li, C.; Tao, Y.; Ao, W. Improving forecasting accuracy of daily enterprise electricity consumption using a random forest based on ensemble empirical mode decomposition. *Energy* **2018**, *165*, 1220−1227.